ELSEVIER

Sensors and Actuators A 52 (1996) 86–91

SENSORS AND ACTUATORS A PHYSICAL

A laterally driven micromachined resonant pressure sensor

Christopher J. Welham [a], Julian W. Gardner [a,*], John Greenwood [b]

[a] *Department of Engineering, University of Warwick, Coventry CV4 7AL, UK*

[b] *Druck Ltd, Fir Tree Lane, Groby, Leicester LE6 OFH, UK*

Abstract

A new type of resonant pressure sensor is presented which employs a laterally driven resonant strain gauge. The resonant strain gauge is designed using simple linear elastic theory and the sensor fabricated by a combination of bulk- and surface-micromachining techniques. The strain gauge is driven electrostatically and the resultant vibration sensed capacitively. Its lateral mode of oscillation offers several advantages, such as a Q-factor insensitive to the leakage of cavity gases. The resonator has been designed to have a fundamental frequency of 52 kHz and a gauge factor of 60 Hz μN^{-1}. Preliminary measurements of devices yield a fundamental frequency of 52 ± 15 kHz, a Q-factor in air of 50 and a pressure sensitivity of 8.8 kHz bar^{-1}.

Keywords: Micromachining; Polysilicon; Resonance; Pressure sensors

1. Introduction

Conventional ultra-high-precision pressure sensors employ resonant strain gauges to convert a pressure-induced diaphragm strain into a frequency shift. The advantage of this structure is that the resonator is very sensitive to the applied strain (pressure) and so the output frequency can be measured very precisely. Thus, high resolution (ca. ppm) and pressure sensitivity can be attained. Moreover, sinusoidal signals are less susceptible to noise and interference and electronic integration is simplified. Applications for these precision sensors include calibration, automotive, medical, aerospace, military, process and industrial control and HVAC (heating ventilation and air conditioning) [1]. Resonant pressure sensors consist of a resonant element attached to one or more diaphragms, although the integration of the diaphragm and resonator into a single element is possible [2]. These sensors are, however, generally fabricated using bulk silicon processing techniques (such as anisotropic etching, etch-stops and silicon fusion bonding [3–5]), which restricts the resonator design, giving rise to several disadvantages. First, the drive force is non-linear. Secondly, the Q-factor is very sensitive to gas levels in the cavity. Thirdly, a boron etch-stop introduces high internal stresses, which preclude the use of thinner structures that provide a higher strain sensitivity.

In this paper we describe the design, fabrication and initial testing of a new type of resonant pressure sensor based on a lateral resonant strain gauge. One major advantage of a lateral-mode resonator is that the Q-factor is less dependent on the cavity pressure due to a smaller gas-damping coefficient and so should have a better long-term stability. Moreover, a linear excitation force–displacement relationship is possible, and the mechanical coupling between the diaphragm and resonator is minimized as their fundamental resonant modes are perpendicular. The pressure sensor is fabricated by combining surface- and bulk-micromachining processes, which enables greater flexibility of design.

2. Design

The pressure sensor consists of a laterally driven micromachined resonant strain gauge mounted centrally on a single-crystal silicon (SCS) diaphragm. Under an applied pressure the diaphragm deflects, rotating and translating the flexure anchor points, see Fig. 1(a). The force applied to the flexure induces a change in the fundamental frequency of the resonator. The resonator, fabricated from polysilicon, consists of an inertial mass supported by four beams 150 μm long, forming a hammock-type flexure. The resonator is excited electrostatically, and motion sensed capacitively, via two 25-plate comb capacitors, see Fig. 1(b).

The fundamental frequency of the resonator is calculated using Rayleigh's method, for small vibration amplitudes

* Corresponding author. Tel: +44-1203-3523695. Fax: +44-1203-418922. E-mail: j.w.gardner@warwick.ac.uk.

SSDI 0924-4247(96)01118-1

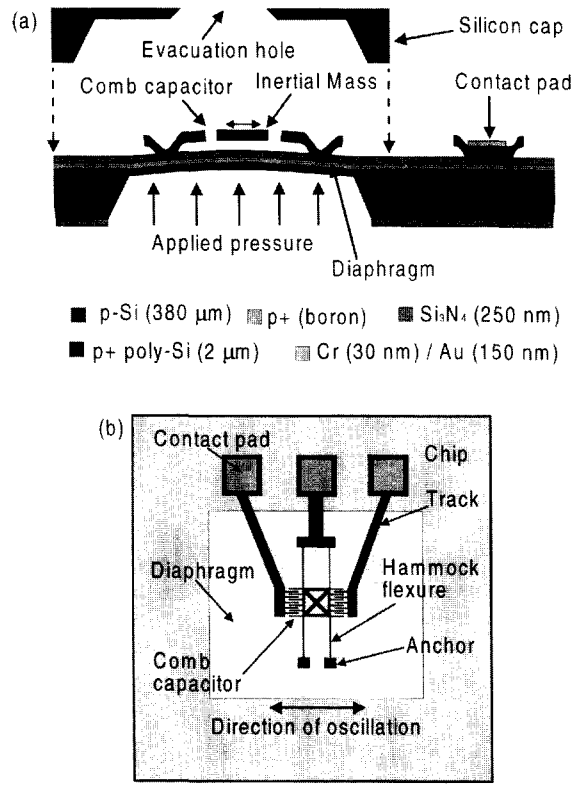

Fig. 1. (a) Schematic cross section and (b) plan view of lateral resonant pressure sensor.

where the spring rate is approximately linear. An extra potential strain energy term is included to determine the sensitivity to a tension, T, applied laterally to the flexure. For the resonator shown in Fig. 1(a) and (b) the fundamental frequency, ω_0, is approximately given by

$$\omega_0 \approx \sqrt{\frac{24}{5L^3}\left[\frac{10EI+TL^2/4}{M_I+13M_B/35}\right]} \tag{1}$$

where the inertial mass, M_I, is supported by flexure of mass M_B, length L and flexural rigidity EI. An expression for the tension sensitivity, or gauge factor, is calculated by differentiating Eq. 1:

$$\frac{d\omega_0}{dT} \approx \sqrt{\left[\frac{3L}{40(M_I+13M_B/35)(10EI+TL^2/4)}\right]} \tag{2}$$

The resonator is designed to have a fundamental frequency of 52 kHz and has a gauge factor of about 60 Hz μN^{-1} for small tensile forces (in the micronewton range). The relatively low fundamental frequency simplifies the integration of the sensor electronics.

The spring rate of the hammock flexure is non-linear (unlike lateral resonators employing folded, crab leg, serpentine or spiral flexures) and gives rise to the characteristic bending of the frequency response (and phase response) seen in resonant pressure (or force) sensors. The non-linear transfer function of the resonator may be obtained by solving the non-linear differential equation describing the dynamics of the resonator. If the non-linear spring rate of the hammock flexure is assumed to be cubic this equation takes the form

$$\ddot{x}+\frac{c}{M_I}\dot{x}+\omega_0{}^2x+\frac{\beta x^3}{M_I}=\frac{F_D}{M_I}\cos(\omega t+\phi) \tag{3}$$

where the inertial mass, M_I, is supported by a hammock flexure that possesses a restoring force $kx+\beta x^3$ where x is the displacement of the inertial mass from equilibrium. The inertial mass is driven by a force of magnitude F_D and its motion damped by a force equal to $c\dot{x}$, where c is the damping constant. The periodic solutions of Eq. (3), known as Duffing's equation, may be obtained by iteration. An initial solution of the form $X_0 = A\cos\omega t$ is assumed and substituted into Eq. (3), eventually leading to a relation between F_D, A and ω [6,7]:

$$\left[(\omega_0{}^2-\omega^2)A+\frac{3\beta}{4M_I}A^3\right]^2+\left[\frac{c\omega A}{M_I}\right]^2=\left[\frac{F_D}{M_I}\right]^2 \tag{4}$$

The amplitude of vibration, A, is calculated for a prescribed excitation frequency by calculating the real roots of Eq. (4). Fig. 2 shows a set of solutions, computed using MATLAB©, that trace the envelope of the non-linear transfer function. The loci of the horizontal and vertical tangents of the response are calculated by implicit differentiation of Eq. (4). At the intersection of the loci with the transfer function the amplitude (and phase) jump to a new level, depending on the direction of the frequency sweep as indicated at points A and B in Fig. 2. A linear mechanical transfer function, calculated using lumped system analysis, is included as a comparison. The analysis assumed an excitation amplitude of 120 V, a Q-factor of 50 and a linear spring rate, k, of 7.0 N m^{-1}. The non-linear spring rate β was set to a value 1×10^{10} N m^{-1}

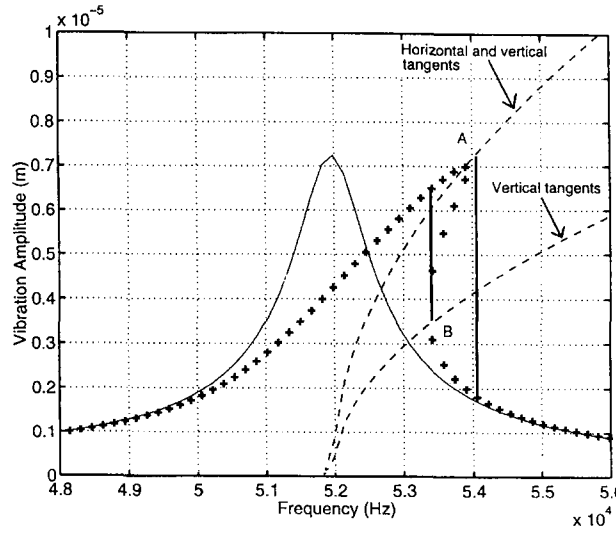

Fig. 2. Linear (continuous line) and non-linear mechanical transfer function (outlined by crosses) for the hammock-type flexure resonator. Depending on the direction of the frequency sweep, the amplitude of vibration 'jumps' to a new level. The 'jump' occurs at the intersection of the horizontal and vertical tangents (dashed lines) with the non-linear transfer function, at points A and B, in the direction indicated.

based upon the hysteresis interval observed experimentally (see Section 4).

2.1. Excitation and signal detection

The resonator may be operated in either a one-port or two-port configuration. In a one-port configuration the resonator is excited electrostatically from both sides (push–pull mode) and its resonance detected by an impedance shift. In a two-port configuration the motion is sensed by applying a bias voltage to the sense comb and measuring the current generated by the time-varying sense capacitance. As the electrostatic drive force is a function of the square of the drive voltage it is possible to excite the resonator with an anharmonic frequency that is equal to half the fundamental frequency, although higher excitation voltages are needed. The two-port electromechanical transfer function is calculated using lumped system analysis, from which the magnitude of the sense current is given by [8]

$$|i_s| \approx \frac{(dC/dx)^2 V_s V_p V_d Q}{M_1 \omega_0} \quad (5)$$

where the inertial mass M_1, biased with a voltage V_p, is driven by a sinusoid of frequency ω_0 and magnitude V_d. The constant dC/dx is a function of the comb capacitor dimensions, V_s is the d.c. bias applied to the sense comb and Q the Q-factor. For a V_s of 20 V, V_p of 20 V, V_d of 5 V and an estimated Q-factor of 50 000 in vacuum, a sense current of about 20 nA at resonance is predicted. Amplification of the sense current is achieved with a virtual earth transimpedance amplifier.

2.2. Electrical crosstalk

Electrical crosstalk between the drive and sense ports due to resistive and capacitive coupling can decrease (and possibly mask) both the maximum phase shift and relative change in magnitude of the two-port electromechanical transfer function. (In the one-port mode parasitic parallel loads can obscure the mechanical resonance [9].) Electrical crosstalk may be reduced by using an anharmonic drive signal, modulating the sense current with a high-frequency carrier, increasing the resistance of the crosstalk path and integrating a second (reference) resonator adjacent to the pressure-sensitive resonator. By comparing the output of each resonator, the effects of crosstalk, ambient temperature variation and packaging stress are reduced, and the calibration accuracy improved.

3. Fabrication

The sensor was fabricated at the University of Twente (The Netherlands) from a combination of bulk and surface micromachining. First, a ground plane is formed by standard boron diffusion into a <100> p-type silicon wafer (double-sided polished). Next, a 250 nm layer of LPCVD low-stress (silicon rich) nitride is grown as an insulation layer (front-side) and anisotropic etch mask (back-side). The etch mask is defined by photo-engraving the back-side nitride with a CHF_3/O_2 plasma. Rectangular, 20 μm thick, SCS diaphragms (and wafer snapping grooves) are then formed using a timed anisotropic KOH etch. Following the anisotropic etch the front-side nitride is photo-engraved in a CHF_3/O_2 plasma to open contact windows to the ground plane, Fig. 3(a).

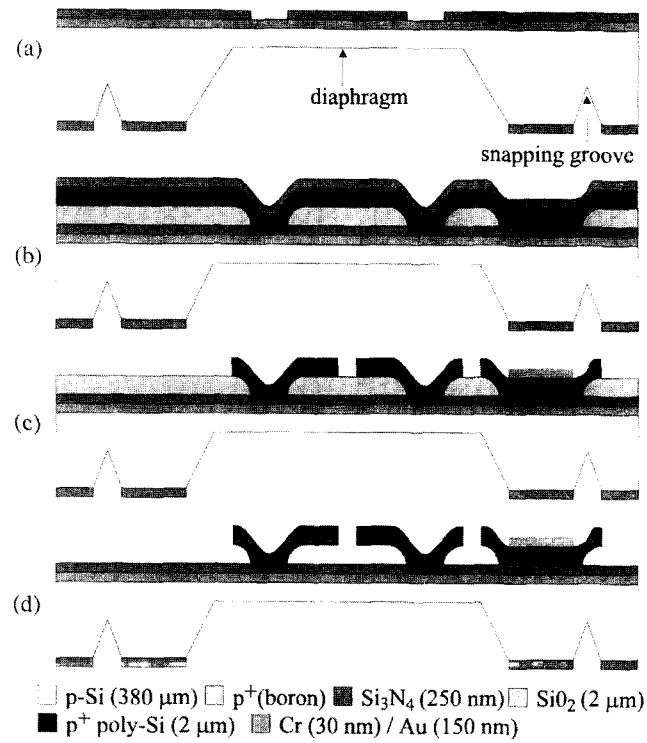

Fig. 3. (a) Diffuse boron and grow Si_3N_4. Photo-engrave back-side Si_3N_4 and etch diaphragms. Photo-engrave front-side Si_3N_4. (b) Grow sacrificial oxide and photo-engrave; deposit α-silicon and BSG then anneal and strip BSG. (c) Deposit and pattern Cr/Au contact pad electrodes. Pattern and dry etch p^+ poly-Si resonator, tracks and pads. (d) Remove sacrificial layer by HF etch and freeze dry.

A 2 μm sacrificial oxide layer is then grown by PECVD, and densified in N_2 at 800 °C to improve the thermal stability. Electrical and flexure contact windows are etched in the oxide using BHF and a photoresist mask. After cleaning, a 2 μm layer of amorphous silicon is grown by LPCVD at a temperature of 590 °C. A dopant source is then created by growing a borosilicate glass (BSG) oxide sandwich by APCVD onto the amorphous silicon. The BSG/oxide layer is then densified at 650 °C for 30 min and the wafer annealed at 1000 °C for 1 h in a nitrogen ambient. During the anneal low-strain polysilicon is formed via crystal growth in the amorphous silicon and, at the same time, the layer is doped as boron atoms diffuse into the silicon. Following the anneal the BSG/oxide sandwich is removed with BHF, see Fig. 3(b).

Metallization of the contact pads is achieved by depositing a chromium–gold sandwich onto a lift-off mask by resistive

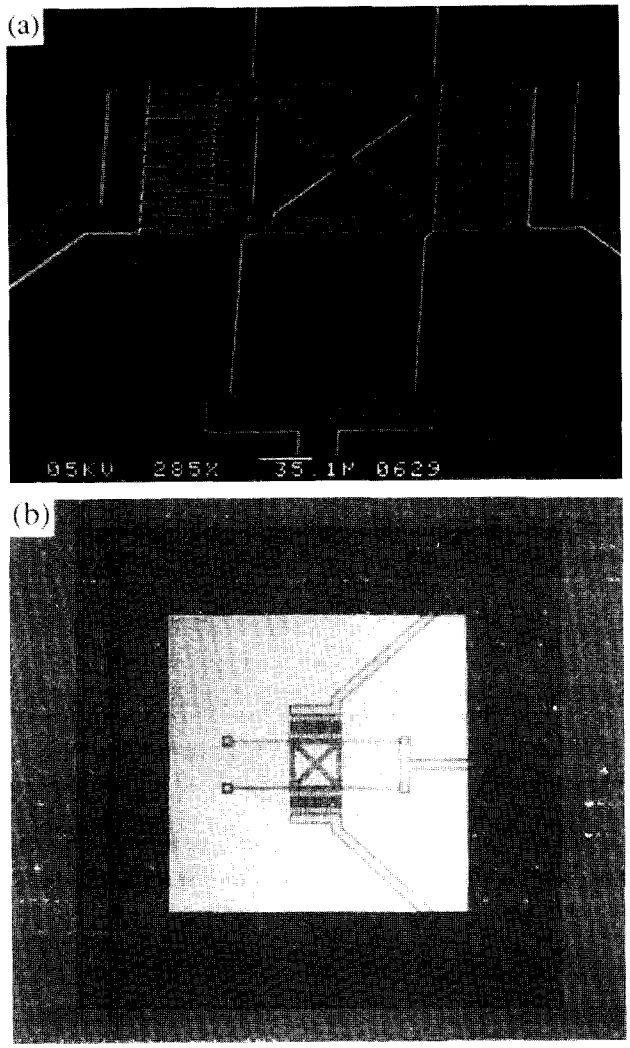

Fig. 4. (a) Micrograph of polysilicon resonator showing inertial mass, hammock flexure and interdigitized comb capacitors. (b) Infrared photograph of microresonator and tracks mounted centrally onto a 20 μm thick single-crystal silicon diaphragm.

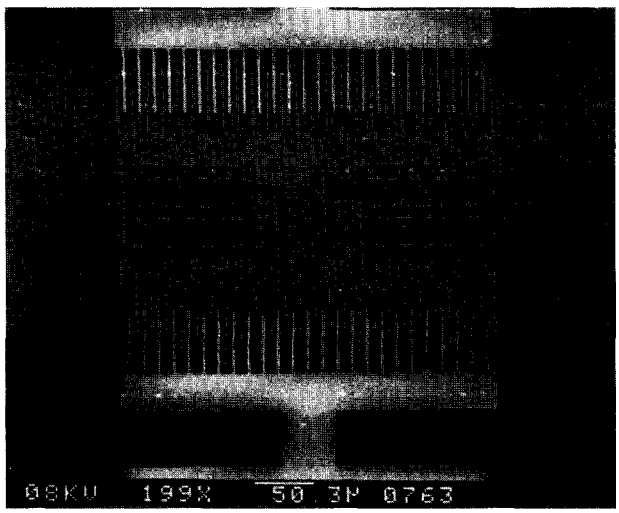

Fig. 5. Micrograph of a microresonator employing 150 μm long folded flexures that possesses a fundamental frequency insensitive to applied strain, used to calculate Young's modulus of polysilicon.

evaporation. Removing the lift-off mask with acetone leaves a metal electrode on the contact pad. The resonator, tracks and contact pads are then defined with photoresist and the polysilicon anisotropically etched in an SF_6/O_2 plasma, see Fig. 3(c). The final step is to free the microstructures by removing the sacrificial oxide with a 1:1 solution of HF (50%). To prevent stiction of the resonators to the substrate, the HF solution is diluted with deionized water and the wafer repeatedly rinsed in IPA, then cyclohexane. The cyclohexane is removed by freeze drying, see Fig. 3(d).

Fig. 4(a) shows a micrograph of the resonant strain gauge and Fig. 4(b) shows an infrared photograph of the resonator and diaphragm. The residual strain in the annealed polysilicon is measured using an array of micro-rotational strain gauges [10]. From measurements of the deflection of the gauge the residual tensile strain in the annealed polysilicon is estimated to be 0.03%.

4. Testing and results

The fundamental frequency is initially measured by observing the vibration resonator under a optical microscope. Fig. 5 shows an SEM micrograph of a resonator employing folded flexures which has a fundamental frequency, independent of residual strain, of about 44 kHz. The fundamental frequency of this resonator is given by

$$\omega_0 \approx \sqrt{\frac{24EI}{L^3(M_1 + 13M_B/35)}} \tag{6}$$

where the constants have been defined earlier. A value for the Young's modulus of polysilcon is obtained from Eq. (6), as the fundamental frequency is known, and in this case is about 195 GPa.

The pressure sensor is mounted onto a carrier chip and the assembly attached to a glass tube connected to a calibrated pressure line. The resonator shown in Fig. 6 (at $\times 600$ mag-

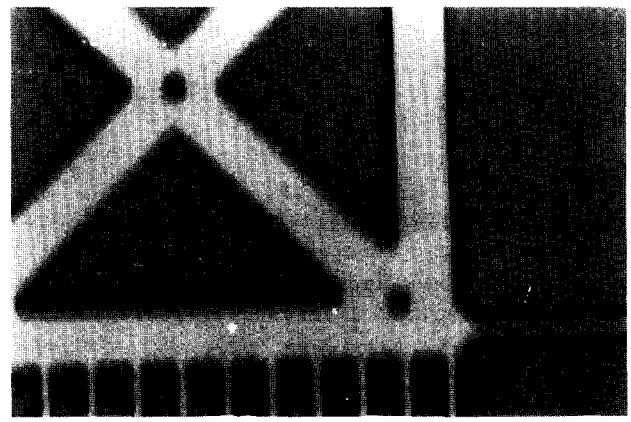

Fig. 6. Photograph ($\times 600$ magnification, reduced in reproduction 80%) of microresonator shuttle and flexure arm, excited by 120 V anharmonic drive signal vibrating at ≈ 57 kHz. The amplitude vibration envelope is determined by comparison with the comb finger width (3 μm) and is approximately 6 μm.

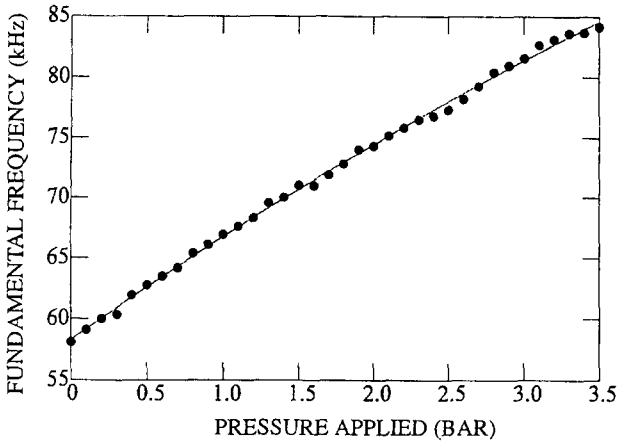

Fig. 7. Variation in fundamental frequency with applied pressure at 19.5 °C (error bars are omitted for clarity but are typically 1–2%).

nification, reduced in reproduction 80%) is excited by applying a sinusoidal drive signal of 40 V amplitude to the drive comb and biasing the ground plane and sense comb with a fixed potential of 90 V. Alternatively, a drive force of equal magnitude is created by applying an anharmonic drive sinusoid of 120 V amplitude to the drive comb while grounding the inertial mass and sense comb. The fundamental frequency is found by obtaining the maximum vibration amplitude and is typically within ± 15 kHz of the designed value of 52 kHz. The difference between the designed and actual resonance frequency is due to the residual strain in the polysilicon. Under the bias conditions given above a vibration amplitude of 6 μm was observed, which is in good agreement with the theory. The measured hystereris at this vibration amplitude is about 500 Hz. The Q-factor is measured visually by estimating the frequency at which the amplitude of the envelope falls by 70%, and is about 50 for this resonator in air. However, obtaining an accurate value for the Q-factor in air is problematic as at large vibration amplitudes the transfer function is non-linear. In vacuum a Q-factor of about 50 000 is expected [11].

The variation of the fundamental frequency with applied pressure is shown in Fig. 7. A second-order polynomial of the form

$$f = C_0 + C_1 P + C_2 P^2 \quad (7)$$

is fitted to the experimental data and shows an excellent fit with the correlation coefficient having a value of 0.9992. The linear pressure sensitivity is given by C_1 in Eq. (7) and was found to have a value of approximately 8.82 kHz bar^{-1}.

5. Conclusions

A novel type of silicon pressure sensor based upon a lateral resonator has been successfully fabricated by a combination of bulk- and surface-micromachining techniques. The use of surface micromachining circumvents the design limitations of conventional bulk-micromachined resonators. For example, the straight-forward integration of a dual resonator configuration can reduce the sensitivity of the pressure sensor to variations in both temperature and packaging stress and electrical crosstalk. The main advantage of this type of pressure sensor is a reduction in the sensitivity of the Q-factor to cavity gas levels, which should increase its long-term stability. A disadvantage is that the small gap between the resonator and diaphragm will limit the operating range of the sensor. The small motional capacitance and the effect of crosstalk can also make signal detection problematic.

Initial results show that the pressure sensor has a sensitivity of 8.8 kHz bar^{-1} and a Q-factor of about 50 in air. Work is underway to integrate drive and sense electronics and operate the sensor in a closed-loop mode and to characterize its long-term stability for possible commercial application.

Acknowledgements

The authors are grateful to the MESA Department (University of Twente) for help in device fabrication and in particular to H.V. Jansen, M.J. de Boer, E. Berenschot and M. Elwenspoek. The authors would like to thank Druck Ltd for technical and financial support and the Engineering and Physical Research Council (EPSRC) for funding the CASE studentship.

References

[1] H. Tilmans, Micromechanical sensors using encapsulated built in resonant strain gauges, *Ph.D. Thesis*, University of Twente, The Netherlands, 1993.

[2] E. Stemme and G. Stemme, A balanced resonant pressure sensor, *Sensors and Actuators, A21–A23* (1990) 336–341.

[3] K. Ikeda, H. Kuwayama, T. Kobayashi, T. Watanabe, T. Nishikawa, T. Yoshida and K. Harada, Three dimensional micromachining of silicon pressure sensor integrating resonant strain gauge on diaphragm, *Sensors and Actuators, A21–A23* (1990) 1007–1010.

[4] J. Greenwood, Etched silicon vibrating sensor, *J. Phys. E: Sci. Instrum., 17* (1984) 650–652.

[5] R. Buser and N. de Rooij, Silicon pressure sensor based on a resonating element, *Sensors and Actuators A, 25–27* (1991) 717–722.

[6] J. Stoker, *Non-linear Vibrations in Mechanical and Electrical Systems*, Interscience, New York, 1963, pp. 81–117.

[7] W. Thomson, *Theory of Vibration with Applications*, Unwin Hyman, London, 1988, pp. 7392–7410.

[8] W. Tang, Electrostatic comb drive for resonant sensor and actuator applications, *Ph.D. Thesis*, University of California, Berkeley, 1990.

[9] C. van Mullem, H. Tilmans, A. Mouthaan and J. Fluitman, Electrical cross talk in two port resonators — the resonant silicon beam force sensor, *Sensors and Actuators A, 31* (1992) 168–173.

[10] B. van Drieenhuizen, J. Goosen, R. French and R. Wolffenbuttel, Comparison of techniques for measuring compressive and tensile stress in thin films, *Sensors and Acuators A, 37–38* (1993) 756–765.

[11] W. Tang, T. Nguyen and R. Howe, Laterally driven polysilicon resonant microstructures, *Sensors and Actuators, 20* (1989) 25–32.

Biographies

Chris Welham has a B.Eng. in electronic engineering. He is currently a research student in the Department of Engineering at the University of Warwick on a Ph.D. programme supported by the Engineering and Physical Research Council and sponsored by Druck Ltd.

Julian Gardner is a reader in the Department of Engineering at the University of Warwick. He is also director of the Sensors Research Laboratory, which is part of the Centre for Nanotechnology and Microengineering. His research interests include chemical silicon sensors, electronic noses, intelligent sensor systems and pattern-recognition techniques.

John Greenwood has been working for Druck Ltd for about five years and was responsible for introducing a resonant pressure sensor based on bulk silicon micromachining and boron etch-stop. Before this he was with STL in Harlow, Essex (now BNR Europe), where he spent a considerable amount of time developing silicon resonant sensors and micromaching techniques, including the discovery of the boron etch stop. He was awarded a B.Sc. in chemistry in 1965 and holds a number of patents relating to mechanical devices.